Journal of Materials Chemistry A

Accepted Manuscript

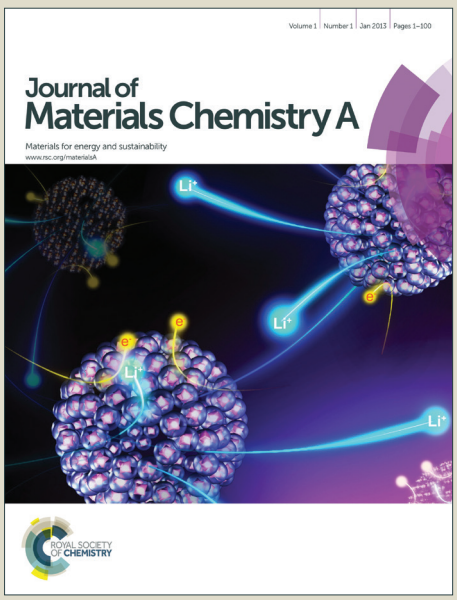

ROYAL SOCIETY OF CHEMISTRY

www.rsc.org/materialsA

Water-dispersible Fe_3O_4 nanowire as efficient support for noble-metal catalysed aqueous reactions

Cite this: DOI: 10.1039/x0xx00000x

Yujiao Jiang[a,b], Guozhu Li[a,*], Xiaodi Li[a], Shuxiang Lu [b,*], Li Wang[a], and Xiangwen Zhang[a]

Received ooth January 2012,
Accepted ooth January 2012

DOI: 10.1039/x0xx00000x

www.rsc.org/

Water-dispersible magnetic Fe_3O_4 nanowire was synthesized at room temperature by coprecipitation method using bio-inspired dopamine as shape-directing surfactant. The as-synthesized nanowire was used to load noble metal (Pd and Pt) for the preparation of magnetic nanocatalysts. The Fe_3O_4-nanowire supported noble metal exhibits bi-functional properties with stable water dispersion and excellent catalytic activity toward the hydrogenation of 4-nitrophenol and reduction of 4-nitrophenol by $NaBH_4$ in water. In addition, the magnetic heterostructured nanocatalysts show good separation ability and reusability for at least 5 successive cycles. Moreover, the Pd/Fe_3O_4 nanowire can also act as an efficient catalyst for the Suzuki reaction under aqueous condition.

Introduction

Supported-metal catalysts are among the most important materials in heterogeneous catalysis.[1-4] Many industrial catalysts consist of noble metals dispersed on high-area porous supports. Their catalytic performance strongly depends on the chemical nature and physical structure of the supports.[5-9] Generally, metal-support interaction (MSI) plays an important role in determining the catalytic performance via affecting the size and chemical states of metal nanoparticles.[5, 10]

Low-dimensional oxide supports have attracted much attention over the past decade because of both their specific exposed crystal planes and interesting physical properties. One-dimension CeO_2 has been widely used as support for catalytic applications.[11-14] Gao et al.[15] showed that ZrO_2-CeO_2 nanorods achieved a significantly better performance than its nanocubes and nanopolyhedra as support for the selective catalytic reduction of NO with ammonia. Mou and coworkers[16] studied γ-Fe_2O_3 nanorods, which preferentially expose the reactive facets by crystal-phase and morphology control through a solution-based approach, efficiently catalyse selective reduction of NO with NH_3. Zhong et al.[17] prepared Au/α-Fe_2O_3 nanorod catalyst exhibiting higher catalytic activity than the commercial available Au/α-Fe_2O_3. Qiu et al.[8] successfully synthesized NbC nanowires as efficient support of platinum for methanol oxidation reaction. Wang et al.[18] demonstrated that copper nanoparticles dispersed rod-shaped $La_2O_2CO_3$ can efficiently catalysed transfer dehydrogenation of primary aliphatic alcohols with an aldehyde yield of up to 97%. In addition, TiO_2-based nanowire was investigated by Park and colleagues as support for methanol electrooxidation in direct methanol fuel cells.[19] Rajeswari et al.[20] reported the use of tungsten trioxide nanorods as supports for platinum in methanol oxidation.

Magnetite is an ideal oxide support, easy to prepare, having a very active surface for adsorptions or immobilization of metals and ligands, which can be separated by magnetic decantation after the reaction.[21-23] Anisotropic magnetic nanomaterials are expected to exhibit unique properties, so one-dimensional (1D) magnetite nanostructures have been the focus of considerable interests. Although substantial efforts has been devoted to the design and controlled fabrication of 1D magnetite nanostructures, it is still difficult to directly prepare magnetite with 1D nanostructure owing to the complexity of its spinel structure. Up to now, only little work is related to the preparation of 1D magnetite nanostructures, among which template-assisted method[22, 24, 25], hydrothermal treatment of the precursor[26-28], magnetic-field-induced growth route[29] and microemulsion-based method[30] are main. Therefore, development of a simple, green and cost-effective method for fabricating 1D magnetite nanostructures is still highly desirable.

Herein, we report a convenient room-temperature preparation route for single-crystalline Fe_3O_4 nanowires in aqueous solution, in which mussel-inspired dopamine has been selected as shape-directing agent. The as-synthesized magnetic and water-soluble Fe_3O_4 nanowire was used as support to load noble metal nanoparticles. To evaluate the activity and the stability of the nanocatalysts, the hydrogenation of 4-nitrophenol (4-NP), reduction of 4-NP by $NaBH_4$ and Suzuki-Miyaura coupling reaction in water were selected as the model reactions.

Experimental

Preparation of water-soluble magnetic Fe_3O_4 nanowire

Fe_3O_4 nanowire was synthesized at room temperature using dopamine as capping agent. Briefly, 0.583 g of $FeCl_3.6H_2O$ and 0.212 g of $FeCl_2.4H_2O$ were dissolved in 8ml of distilled water. Certain amount of dopamine was dissolved in 2ml of distilled water. Then the dopamine solution was added dropwise to the iron salt mixture at N_2 atmosphere. The mixture was stirred vigorously for 1 h to make all materials dissolved completely. Then NaOH solution (5M) was used to adjust the pH of the solution to 10. The reaction mixture was stirred vigorously for 30 min under N_2 protection. During this process, it was observed that the originally dark green solution changed to

black indicating the formation of Fe_3O_4 and completion of the reaction.

Synthesis of Fe_3O_4-nanowire supported Pd (or Pt)

89 μL of 56.4 mM H_2PdCl_4 (or 67 μL of 75 mM H_2PtCl_6) solution, 2ml of the above as-synthesized Fe_3O_4 solution, and 2.9 ml of distilled water were pre-prepared in a vial. The final volume of all reaction solutions was 5 ml. The reaction mixture was stirred vigorously for 30 min at N_2 atmosphere. Due to the reducibility of dopamine, no reducing agent was used.

Synthesis of Pd (or Pt) nanoparticles

1 mM H_2PdCl_4 (or H_2PtCl_6), and 2 mM ascorbic acid were prepared in a vial, and one shot of $NaBH_4$ with a final concentration of 0.8 mM was injected. The final volume of all reaction solutions was 5 ml. The reaction mixture was stirred vigorously for 30 min at N_2 atmosphere.

Catalytic Reactions

The obtained nanocatalysts were used to catalyse two model reactions, the reduction of 4-NP by $NaBH_4$ (Scheme S1) and hydrogenation of 4-NP (Scheme S2), to evaluate their catalytic performance.

4-NP reduction by $NaBH_4$: The reduction of 4-NP by the nanocatalyst in the presence of $NaBH_4$ was carried out to examine its catalytic activity and recyclability (Scheme S1). Amounts of 3 mL of 0.1 mM 4-NP, and 10 μL of 3 M $NaBH_4$ solutions were added into a quartz cuvette followed by addition of catalyst solution to the mixture. For the nanoparticle catalysts, the final concentration of noble metal (Pd and Pt) is 3.3×10^{-6} mol/L. For the supported catalysts, the final concentration of Pd/Fe_3O_4 (or Pt/Fe_3O_4) catalyst is 0.034 g/L. As calculated by ICP data, the amount of noble metal from the supported catalyst in the solution is 0.30 mg/L for Pd or 0.18 mg/L for Pt. The color of the solution changed gradually from yellow to transparent as the reaction proceeded. UV-Vis spectrometry was used to record the change in absorbance at a time interval of 1s at λ=400nm. Therefore, a U3010 spectrophotometer was employed to monitor the progress of the conversion of 4-NP to 4-aminophenol (4-AP) at ambient temperature.

Hydrogenation of 4-NP: The simplified schematic diagram of hydrogenation of 4-NP is shown in Scheme S2. The hydrogenation reaction was carried out in an 80 mL custom designed stainless autoclave with a Teflon inner layer at room temperature. In a typical procedure, certain amount of catalyst was dispersed in 60 mL of 0.1 mM 4-NP. The final concentration of noble metal (Pd and Pt) nanoparticle is 3.3×10^{-6} mol/L. The final concentration of Pd/Fe_3O_4 (or Pt/Fe_3O_4) catalyst is 0.034 g/L. As calculated by ICP data, the amount of noble metal from the supported catalysts in the solution is 0.30 mg/L for Pd or 0.18 mg/L for Pt. The reactor was sealed, purged with hydrogen and pressurized to 0.4 MPa. The reaction mixture was stirred with a magnetic stirrer at a rate of 300 rpm at room temperature. A constant pressure of 0.4 MPa was maintained throughout the reaction course by supplying hydrogen from a Hydrogen Generator (GCH-300). The reactants were analyzed by UV-Vis spectrometry.

Suzuki-Miyaura coupling reaction: Iodobenzene (204 mg, 1.0 mmol) was added to a stirred mixture of SDS (144 mg, 0.5 mmol), tripotassium phoshate (K_3PO_4, 399 mg), phenylboronic acid (146 mg, 1.2 mmol), and deionized water (H_2O) (20 mL), followed by Pd/Fe_3O_4 nanowire catalyst (0.366 mg/L Pd). The mixture was then stirred at certain temperature in N_2 atmosphere. After reaction, the mixture was taken out and then extracted with ethyl acetate (3 × 20 mL). The combined organic extract was dried over anhydrous sodium sulfate (Na_2SO_4), and the resulting mixture was analyzed by gas chromatography (Bruker 456), equipped with an FID (flame ionization detector) and a commercially column (ZB-5, 30 m × 0.32 mm × 0.1μm).

Characterization

The crystal structures were recorded using a Rigaku D/max-2500 X-ray diffractometer (XRD) equipped with a Cu Kα irradiation source. The morphology and microstructure were examined on a Tecnai G^2 F20 transmission 100 electron microscopy (TEM) operated at 200 kV and a Nanosem 430 field emission scanning electron microscopy (SEM) with energy-dispersive X-ray spectroscopy (EDS). A Hitachi U-3010 UV-Vis spectrometer using a 1 cm path length quartz cuvette was used to identify the change in concentration at λ=400 nm. The noble metal (Pd and Pt) loading amount was determined by inductively couple plasma-optical emission spectrometry (ICP-OES, VISTA-MPX). Magnetization measurements were carried out using a vibrating sample magnetometer (VSM, LDJ 9600-1) under an applied magnetic field at room temperature. The X-ray photoelectron spectroscopy (XPS) studies were carried out on a PHI 5300 system (PHI), using an aluminum anode (Al Ka, 1486.6 eV) operating at 250 W. The pass energy was 188 eV for the survey scan and 47 eV for the region scan.

Results and discussion

Synthesis of water-dispersible Fe_3O_4 nanowire

Magnetite nanoparticles are commonly produced via coprecipitation of Fe(II) and Fe(III) ions by a base, usually sodium hydroxide or aqueous ammonia.[31] Direct synthesis of Fe_3O_4 nanowires is difficult because of the great difference in deposition rate of Fe(II) and Fe(III) ions in aqueous solution. In addition, the isotropic structure of magnetite has also caused difficulties in anisotropic growth of nanocrystal. Inspired by mussels, catechol-derived molecules have been utilized as high affinity anchors for nanoparticle stabilization. Irena et al.[25] prepared magnetic nanorods using dopamine as shape-control agent at 100 °C. Herein, dopamine has been selected as capping agent for two purposes. First, the catechol structure can specifically interact with iron atom, which has been confirmed by Raman spectroscopy.[32] Second, dopamine will also self-

polymerize to form a coating on the surface in water.[33] Then, the size of Fe_3O_4 can be efficiently controlled by dopamine and interesting nanostructures were supposed to get at room temperature due to the above two interactions and its biomimetic property.

Magnetite samples were obtained by the traditional coprecipitation method and the revised dopamine method (6 g/L dopamine). Figure S1 shows the water solubility of Fe_3O_4 samples from traditional coprecipitation method (left vial) and dopamine-regulated method (right vial). As illustrated in Figure S1(a), both samples were soluble in water at the initial time. But after 3 hours, it is easily observed that Fe_3O_4 solution obtained by traditional method aggregated and precipitated. While the Fe_3O_4 solution regulated by dopamine is still stable without any visible precipitate, which indicates the excellent water solubility of the dopamine-regulated Fe_3O_4.

The crystallinity and phase composition of the resulting products was investigated by X-ray powder diffraction (XRD). The XRD pattern of sample prepared by dopamine regulation is shown in Figure 1. The diffraction peaks at 2θ values of 18.3º, 30.1º, 35.5º, 43.1º, 57.0º, 62.6º, and 74.4º could be indexed to the (111), (220), (311), (400), (511), (440), and (533) crystal planes of Fe_3O_4, respectively. Result confirms that single crystal of Fe_3O_4 has been still obtained with the introduction of some dopamine. The broadening of reflection peaks indicates the formation of ultrafine particles. Therefore, dopamine can effectively control the size distribution of Fe_3O_4 particles.

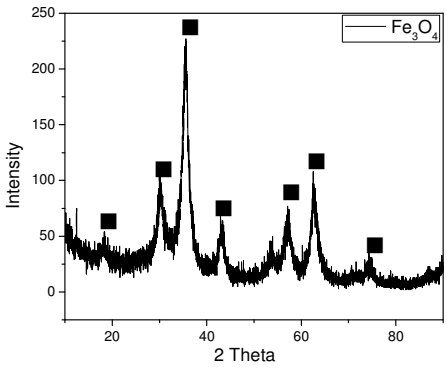

Fig. 1 XRD pattern of the Fe_3O_4 prepared by dopamine regulation.

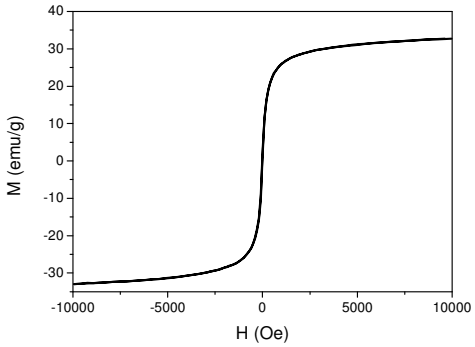

Fig. 2 Hysteresis loops of the as-synthesized Fe_3O_4.

The magnetic properties of the dopamine-regulated Fe_3O_4 were studied using a vibrating sample magnetometer (VSM) at room temperature in the applied magnetic field ranging from -10000 Oe to 10000 Oe. Figure 2 shows the magnetic hysteresis loop of the dopamine-regulated Fe_3O_4. Data demonstrated that the resulting product exhibited a characteristic of ferromagnetism with a saturation magnetization of 33.0 emu/g. The sample also displays typical superparamagnetic behavior with neglectable small hysteresis loop due to its nanometer size. It is noteworthy that the saturation magnetization obtained in this study is much lower than that of bare Fe_3O_4 nanoparticles reported in the literature.[34] The systematic decrease of the saturated magnetization is undoubtedly related to the covered surface of Fe_3O_4 by organic polydopamine.

The effect of dopamine amount in Fe_3O_4 synthesis was further studied. Fe_3O_4 nanoparticles with the size of around 150 nm and polyhedron structure were obtained by traditional coprecipitation method, as shown in Figure S2. Figure 3 shows typical TEM images of Fe_3O_4 regulated by various amount of dopamine. Interestingly, the morphology changed drastically as compared to traditional Fe_3O_4 nanoparticles. We can see that when the final concentration of dopamine was 1g/L, nanosized iron oxide nanoparticles with narrow size distribution were obtained. This is consistent with the XRD result, showing that the addition of dopamine in the coprecipitation process can finely narrow the size distribution of Fe_3O_4 nanoparticles. When the amount of dopamine increased to 2 g/L, uniform nanoparticles with smaller size (5 nm-10 nm) were obtained. Notably, iron oxide nanowire began to appear in the mixture with the length of 7 nm-60 nm and width of 5 nm-8 nm (Figure 3B). The amount of nanowire increased with the increasing of dopamine concentration to 4 g/L. The nanowires are with the size of 27.29 ± 7.46 nm in length and 2.93 ± 0.57 nm in width (Figure 3C, data of 20 counts). But it is still a mixture of nanoparticles and nanowires. When the amount of dopamine was increased to 6g/L, nanowires were mainly obtained after reaction. The Fe_3O_4 nanowires are 33.84 ± 9.49 nm in length, 3.9 ± 1.6 nm in width in average (Figure 3D, data of 20 counts). The size of nanowire is larger in comparison to that of 4 g/L dopamine, which can be explained by the conversion of more iron oxide into nanowires. When the amount of dopamine was

increased to 8 g/L, the magnetic property of the sample was lost duo to the high ratio of organic coating. Therefore, dopamine with the concentration of 6 g/L was selected as reaction condition to synthesize nanowire for the latter usage as support of noble metal.

The crystallographic nature of the Fe_3O_4 nanowires was further examined by HR-TEM. Figure 4 shows typical Fe_3O_4 nanowires growing along the [111] direction. The lattice fringes (0.24 nm in Figure 4B and 4D) along nanowires in the axial direction observed in these images agree well with the separation between the (222) lattice planes. The interplanar distances of 0.21 nm (Figure 4A) and 0.30 nm (Figure 4C) correspond to the lattice fringes of the {100}, and {110} planes, respectively. Figure 4A displays the angle between (400) and the crosssection of nanowire is 54.4°, which is consistent with the angle between (400) and (222). As shown in Figure 4C, it is 35° between (220) and the crosssection of nanowire, which further confirms that the nanowires grow along [111] direction.

In previous studies, [110] is the main direction for the growth of magnetite nanowires.[25-27, 29] In addition, the Fe_3O_4 nanowire will grow along [100] direction when ferrous sulphate is hydrothermally treated with the assistance of polyethylene glycol (PEG) 400.[35] Nanowire growing along [331] direction was obtained by a sol-gel process in the presence of ethylene glycol and poly(ethylene glycol)-block-poly(propylene glycol)-block-poly(ethylene glycol).[36] Herein, the magnetite nanowire growing along the rare [111] direction indicates that biomimetic dopamine has unique shape-directing effect in the synthesis of Fe_3O_4.

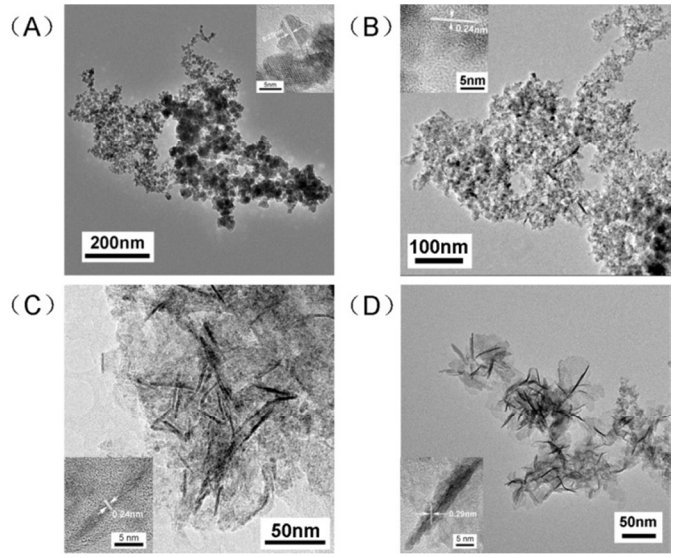

Fig. 3 TEM images of Fe_3O_4 samples regulated by dopamine with the concentration of 1g/L (a), 2g/L (b), 4g/L (c), and 6g/L (d), respectively.

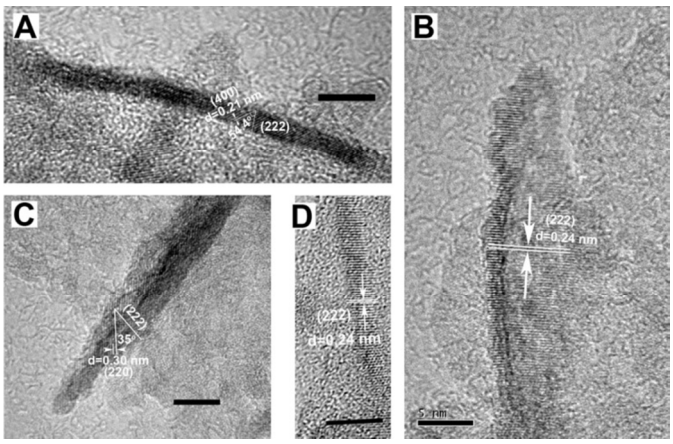

Fig. 4 HR-TEM images of the as-synthesized Fe_3O_4 nanowires (scale bare = 5 nm).

Loading of noble metal on Fe_3O_4 nanowire

Noble metal (Pt or Pd) was then loaded onto the as-synthesized Fe_3O_4 nanowires by simply stirring within metal salt solution at room temperature. It has been reported that polydopamine coating can reduce noble metal ions and grow metal nanoparticles on coating surface due to the metal binding ability of catechols.[37, 38] After loading, both samples (Pd/Fe_3O_4 and Pt/Fe_3O_4) retain the good water stability. As an example, Figure 5 shows the water solubility of Pd/Fe_3O_4. As illustrated in Figure 5a, it is easily observed that a clear and transparent solution was formed after the catalyst was added to water. After two hours, the solution was still stable, as shown in Figure 5b. Figure 5c and Figure 5d display the separation of the catalyst from water using magnetic field force, indicating that the Fe_3O_4-nanowire supported catalyst also has good magnetic property.

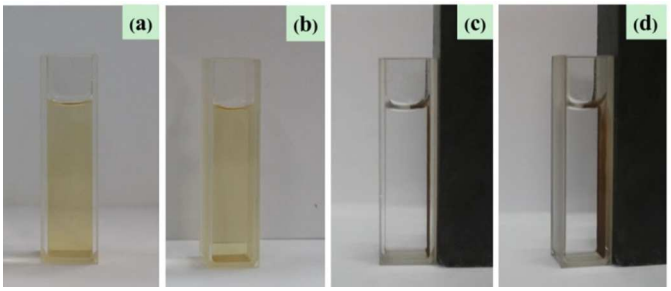

Fig. 5 Photograph of Pd/Fe_3O_4 dispersed in H_2O at initial time (a), two hours later (b) and after magnetic separation (c and d).

Notably, no reflections assignable to metallic Pd (or Pt) were present in the XRD patterns of Pd/Fe_3O_4 and Pt/Fe_3O_4, which is possibly due to the low content of added noble metal. In order to determine the loaded amount of metallic palladium (or platinum) component in the samples, the chemical composition of the products was further analyzed by EDS and ICP tests. As shown in Figure S3 and Figure S4, the compositional analysis carried out by EDS measurements showed the presence of Fe, Pd (or Pt), C, and O elements in the samples. Furthermore, the ICP results also showed that a small amount of Pd (or Pt)

element presented in the samples in addition to Fe element. As calculated by the ICP data, the amount of loaded Pd in Pd/Fe_3O_4 catalyst is 0.90% (wt), and it is 0.53% (wt) of Pt in Pt/Fe_3O_4 sample. Both catalysts showed the existence of loaded noble metal indicating the successful preparation of nanowire-supported catalysts.

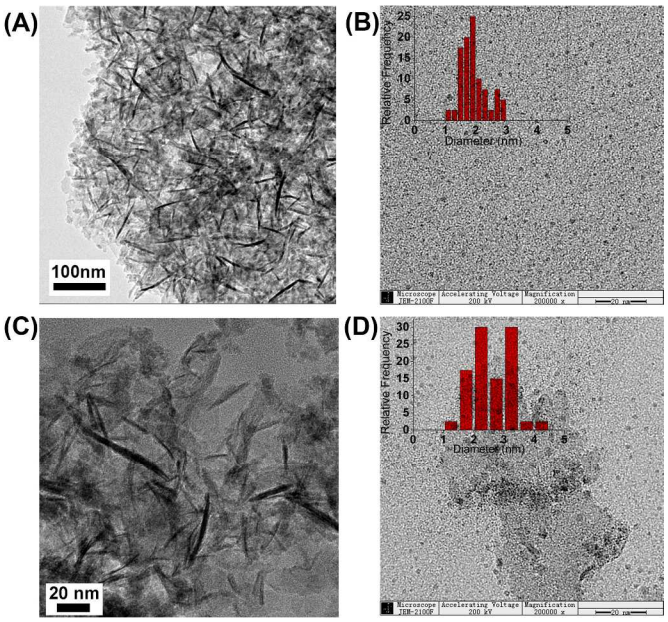

Fig. 6 TEM images of the Fe_3O_4-nanowire supported Pd (A) and Pt (C), and their corresponding particle size distribution (B) and (D) after dissolving Fe_3O_4.

TEM images of the as-synthesized Pd/Fe_3O_4 nanowires and Pt/Fe_3O_4 nanowires are shown in Figure 6(A) and 6(C). After dissolving Fe_3O_4 by hydrocholoride acid, the TEM images and the particle size distribution of Pd and Pt nanoparticles are displayed in Figure 6(B) and 6(C). The average size of Nanoparticles loaded on Fe_3O_4 nanowire is 1.97 ± 0.41 nm (n=20) for Pd and 2.60 ± 0.66 nm (n=20) for Pt.

Nanoparticles of Pd and Pt were selected as the control catalysts, and typical TEM images of the obtained nanoparticles (Pd and Pt) are shown in Figure S5. Pd Nanoparticles with the size of 74.88 ± 11.03 nm (n=19) and Pt nanoparticles with the size of 11.84 ± 5.19 nm (n=50) have been obtained. The corresponding particle size distribution is summarized in Figure S5(C) and (D).

Furthermore, X-ray photoelectron spectroscopy was used to characterize the state of noble metal on the support. Figure S6 and S7 show the XPS survey spectra of Pd/Fe_3O_4 nanowires and Pt/Fe_3O_4 nanowires, respectively.

XPS of Pd(3d) core level region of Pd/Fe_3O_4 nanowires is given in Figure 7. Pd($3d_{5/2}$, $3d_{3/2}$) peaks were resolved into sets of spin-orbit doublets. Accordingly, Pd($3d_{5/2}$, $3d_{3/2}$) peaks are observed at 335.6 eV, 338.1 eV, 340.7 eV and 343.5 eV in the sample. Recent XPS studies[39-41] of Pd metal and PdO show that binding energies of Pd($3d_{5/2}$) in Pd metal, PdO and Pd^{2+} are at 335.4 eV, 336.8eV and 338.2 eV, respectively. Moreover, binding energies of Pd($3d_{3/2}$) are 340.4 eV, 341.6 eV and 343.3 eV for Pd^0, PdO and Pd^{2+}. Thus, Pd($3d_{5/2}$, $3d_{3/2}$) peaks at 335.6 eV and 340.7 eV can be assigned to Pd^0, and 338.1 eV and 343.5 eV peaks can be attributed to Pd^{2+} as in Pd/Fe_3O_4 nanowires. Results indicate that both Pd^0 and Pd^{2+} exist in the catalyst, and Pd^{2+} ions are much more ionic than PdO on nanowire. Relative intensity of Pd(3d5/2) peak of Pd^0 to Pd^{2+} is 0.58.

XPS of the Pt(4f) core level region in the as-prepared Pt/Fe_3O_4 nanowires is displayed in Figure 8. The Pt(4f) region shows four peaks due to double oxidation states in the sample. Hegde et al.[42] have showed that Pt($4f_{7/2}$, $4f_{5/2}$) peaks at 71.0, 74.2; 71.9, 75.1; and 74.3, 77.5 eV could be assigned to Pt metal, Pt^{2+}, and Pt^{4+}, respectively. Thus, in Pt/Fe_3O_4 nanowires the Pt($4f_{7/2}$, $4f_{5/2}$) peaks at 70.5 , 73.9 and 72.1 , 75.8 indicate the existence of Pt^0 and Pt^{2+} in the sample. 70% of Pt is in the form of Pt^0 estimated from the area of the respective XPS peaks.

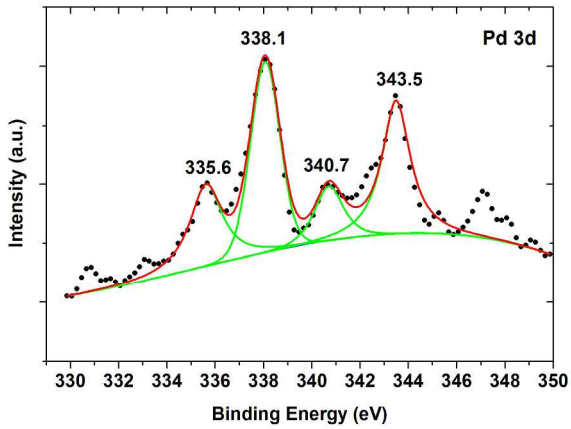

Fig. 7 XPS of Pd(3d) core level region of Pd/Fe_3O_4 nanowires.

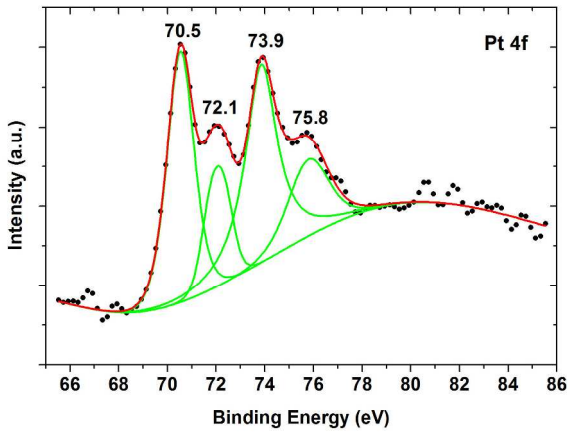

Fig. 8 XPS of Pt(4f) core level region of Pt/Fe_3O_4 nanowires.

Catalytic performance of Fe_3O_4-nanowire supported noble metal

The reductions of 4-NP by $NaBH_4$ and by H_2 have been selected as model reactions (Scheme S1 and S2). Catalytic reduction of 4-NP by borohydride ions is perhaps the most often used reaction to test the catalytic activity of metal nanoparticles in aqueous solution[43]. The reaction take place at the surface of noble metal nanoparticles[44] at room temperature

and can be accurately monitored by UV-Vis spectroscopy. Hence, this model reaction represents cases of heterogeneous catalysis that can be modeled with the accuracy typically available for homogeneous catalysis. Aromatic amines are generally produced by catalytic hydrogenation of nitro compounds. Recently, the hydrogenation of nitro compounds to amines has become one of the most important chemical reactions because organic amines are essential materials for the production of agrochemicals, dyes, pharmaceuticals, polymers and rubbers.[45, 46]

Due to the high concentration of $NaBH_4$, pseudo-first-order kinetics with respect to 4-NP could be used in this case to evaluate the catalytic rate. [43, 47] The absorbencies at λ=400 nm were collected with time in Figure 9(a) and the apparent rate constant can be calculated by linear fitting of the data as shown in Figure 9(b).

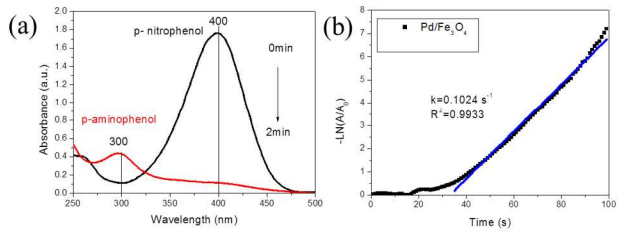

Fig. 9 (a) The absorbance A(t) measured at different times (0 min and 2 min) indicated in the graph is plotted against wavelength in the reduction of 4-NP to 4-AP by $NaBH_4$. (b) Typical time trace of the absorption of 4-NP at 400 nm during their reduction catalysed by Pd/Fe_3O_4. The reaction starts after an induction period t_0, the blue portion of the line corresponds to the linear section, from which rate constant k can be accurately determined. The reaction conditions were as follows: [4-NP]=0.1 mmol/L, [$NaBH_4$]=10 mmol/L, [Pd/Fe_3O_4]=0.034 g/L, and room temperature.

Typical plots of $-\ln(A/A_0)$ against the reaction time for the reactions catalysed by the noble metal nanoparticles and the nanowire-supported catalysts are displayed in Figure 10. As diffusion control can be ruled out, the induction period is caused by processes related to a dynamic substrate-induced surface restructuring of the nanoparticles, which was investigated thoroughly by Ballauff group.[43, 48] For the reactions catalysed by the un-supported noble metal nanoparticles, the average rate constant k is 0.000233 ± 0.000155 s^{-1} (n=5) for Pd nanoparticles and 0.000867 ± 0.000532 s^{-1} (n=5) for Pt nanoparticles, respectively. When the nanowire-supported catalysts were used to catalyse the reaction, the average rate constant k increased to 0.0824 ± 0.0188 s^{-1} (n=5) for Pd/Fe_3O_4 nanowire and 0.0354 ± 0.0071 s^{-1} (n=5) for Pt/Fe_3O_4 nanowire, which is 353 times and 40 times increase in comparison to the corresponding un-supported nanoparticles.

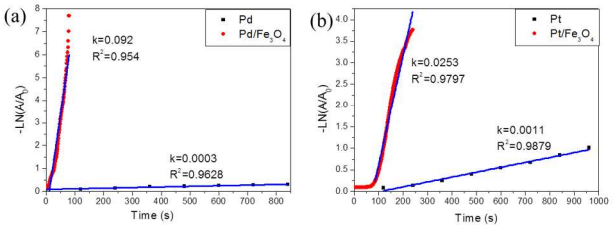

Fig. 10 Typical plots of $-\ln(A/A_0)$ against the reaction time for the reactions catalysed by Pd nanoparticles and Pd/Fe_3O_4 (a) and Pt nanoparticles and Pt/Fe_3O_4 (b). The reaction conditions were as follows: [4-NP]=0.1 mmol/L, [$NaBH_4$]=10 mmol/L, [Pd]= 3.3 × 10^{-6} mol/L for Pd nanoparticles, [Pd]= 2.8 × 10^{-6} mol/L for Pd/Fe_3O_4, [Pt]= 3.3 × 10^{-6} mol/L for Pt nanoparticles, [Pt]= 9.2 × 10^{-7} mol/L for Pt/Fe_3O_4, and room temperature.

For easy comparison of the catalytic performance obtained here and reported previously, the rate constant k was normalized to the surface area of noble metal (m^2/L). The catalytic activity of Pd and Pt reported in the literatures were summarized in Table 1 and Table 2, respectively.

Table 1 Catalytic activity of the Pd nanoparticles for the reduction of 4-NP.

Support	Temp, [°C]	k ($s^{-1}m^{-2}L$)	Reference
Cationic SPB	15	1.1	49
PS-PNIPAM core-shell microgel	15	0.11	49
PAMAM dendrimer	15	0.00307	50
PPI dendrimer	15	0.776	50
PEDOT	25	0.0222	51
Protein	22	0.048	52
Template-free cluster	NA	0.00025	53
Peptide	20	0.027	54
Al_2O_3	25	0.136	55
Poly(ionic liquid) brushes	20	0.58	56
G4-NH_2 PAMAM dendrimer	RT	1.65	57
Fe_xO_y/Pd@$mSiO_2$ composites	RT	0.162	58
Polypyrrole/TiO_2 nanofibers	RT	0.000138	59
Hollow mesoporous @Pd/CeO_2	RT	1.45	60
Template-free	RT	0.0998	This work
Fe_3O_4 nanowire	RT	1.08	This work

Table 2 Catalytic activity of the Pt nanoparticles for the reduction of 4-NP.

Support	Temp, [°C]	k ($s^{-1}m^{-2}L$)	Reference
Cationic SPB	15	0.56	61
PAMAM dendrimer	15	0.0036	50
PPI dendrimer	15	0.0804	50
Organo-silica hybrid nanowires	20	0.31	62
Hybrid macrofibers	RT	0.00235	63
G4-dendrimer/SBA-15 hybrid	25	9.9×10^{-7}	64
Platinum nanonets	20	0.00170	65
Platinum nanonets	30	0.00246	65
Platinum nanoballs	20	0.00229	65
Platinum nanoballs	30	0.00269	65
Template-free	RT	0.057	This work
Fe_3O_4 nanowire	RT	1.83	This work

As displayed in Table 1, the k value of Fe_3O_4-nanowire supported Pd (1.08 $s^{-1}m^{-2}L$) is more than 10 times of the result from unsupported Pd nanoparticles (0.0998 $s^{-1}m^{-2}L$). In Table 2, the high valve of k for the Pt/Fe_3O_4 nanocatalyst (1.83 $s^{-1}m^{-2}L$)

further confirmed the advantage of the Fe_3O_4 nanowire as a support. The rate constant of Pt/Fe_3O_4 here (1.83 $s^{-1}m^{-2}L$) is more than 32 times of k obtained from unsupported Pt nanoparticles, and more than 3.2 times of the other results reported before.

The as-prepared Pd/Fe_3O_4 nanowire and Pt/Fe_3O_4 nanowire heterostructures also show good magnetic properties which can be easily recycled by an external magnet after the catalytic reduction. Figure 11 shows the magnetically recyclable reduction of 4-NP in the presence of Pd/Fe_3O_4 (Figure 11a) and Pt/Fe_3O_4 (Figure 11b) nanocatalysts. Notably, the magnetic nanowire-supported catalysts can be readily recovered from the reaction mixtures by simple magnetic decantation and reused for at least 5 times. However, initial activity drops of 25% for supported Pd and 50% for supported Pt were found due to the loss of unbonded Pd (or Pt).

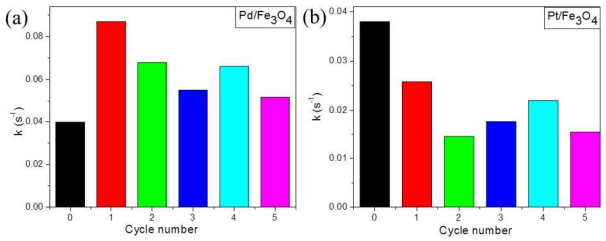

Fig. 11 The values of the rate constant k for each cycle with Pd/Fe_3O_4 (a) and Pt/Fe_3O_4 (b) as catalyst.

Room-temperature hydrogenation of 4-NP to 4-AP in water catalysed by the Fe_3O_4-nanowire supported and un-supported Pd or Pt catalysts is illustrated in Figure 12. The catalytic activities of the Pd (or Pt) catalysts increased dramatically when Pd (or Pt) was loaded on Fe_3O_4 nanowire. When Pd nanoparticles were used as catalyst, the conversion of 4-NP reached 50% in 200 min, and then only little 4-NP was converted. After 705 min, there was still 34% un-converted 4-NP in the solution. While the reaction catalysed by Pd/Fe_3O_4 nanowire gave 100% conversion of 4-NP in 260 min. In comparison to Pd nanoparticles, Pt nanoparticles had better performance (conversion of 84% 4-NP after 11 h). The Pt/Fe_3O_4 nanowire has the best catalytic activity here with 100% conversion of the reactant in only 160 min. Results show that the Fe_3O_4 nanowire is an efficient support for Pt (or Pd) catalysed hydrogenation reaction. Herein, Pt NPs had higher catalytic activity in comparison to Pd NPs for the hydrogenation of 4-NP. While in the reduction of 4-NP by $NaBH_4$, Pd NPs gave better performance (k=0.0998 $s^{-1}m^{-2}L$) than Pt NPs (k=0.057 $s^{-1}m^{-2}L$). Therefore, it can be concluded that the two model reactions have different mechanisms.

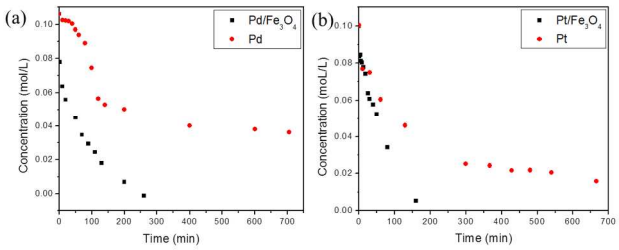

Fig. 12 Hydrogenation of 4-NP catalysed by Pd/Fe_3O_4 nanowire (a) and Pt/Fe_3O_4 nanowire catalyst (b) at room temperature. The reaction conditions were as follows: [4-NP]=0.1 mmol/L, [Pd]= 3.3 × 10^{-6} mol/L for Pd nanoparticles, [Pd]= 2.8 × 10^{-6} mol/L for Pd/Fe_3O_4, [Pt]= 3.3 × 10^{-6} mol/L for Pt nanoparticles, [Pt]= 9.2 × 10^{-7} mol/L for Pt/Fe_3O_4, and at 0.4 MPa of H_2 and room temperature.

Results of catalytic activity obtained here and reported before are summarized in Table S1. Comparable catalytic activity to data reported previously has been obtained using Fe_3O_4 nanowire as a support for the hydrogenation of 4-NP in water at room temperature.

The catalytic activity of the Pd/Fe_3O_4 nanowires in the formation of biaryl carbon–carbon bonds was investigated using the Suzuki reaction of iodobenzene with phenylboronic acid. The catalytic results are summarized in Table 3. By using Pd/Fe_3O_4 nanowire (0.366 mg/L Pd) catalyst, the yield of biphenyl is 14.9% after reaction for 180 min at 18 °C. The biphenyl yield increased to 61.3% after reaction for 60 min at 40 °C.The yield of biphenyl reached as high as 100% after 20 min at 60 °C.

Table 3 Catalytic results for Pd/Fe_3O_4 nanowire under various reaction conditions

Temperature (°C)	Time (min)	Yield (%)
60	20	100
40	60	61.3
18	180	14.9

Conclusions

In this study, uniform water-dispersible Fe_3O_4 nanowires have been obtained at room temperature using a facile modified coprecipitation method. Mussels-inspired dopamine was used as shape-directing agent. The as-synthesized Fe_3O_4 nanowire grows along [111] direction and has a saturation magnetization of 33.0 emu/g. Then, noble metal (Pd or Pt) was loaded on the nanowire to get water-dispersible magnetic nanocatalysts (Pd/Fe_3O_4 nanowire and Pt/Fe_3O_4 nanowire). When the nanocatalysts were used to catalyse the reduction of 4-NP by $NaBH_4$, the rate constant (k, $s^{-1}m^{-2}L$) increased 10 times and 32 times, respectively, in comparison to the un-supported Pd and Pt nanoparticles. In addition, the nanocatalysts can be recycled easily and effectively because of its excellent magnetic property. Experimental results indicated that the catalysts still had good catalytic performance after 5 times recovery and

reuse. Moreover, the Fe_3O_4-nanwire supported Pd and Pt catalysts can efficiently convert all 4-NP to 4-AP by H_2 in 260 min and 160 min, respectively, in water at room temperature. In addition, the resulting Pd/Fe_3O_4 nanowires showed good catalytic activity in the Suzuki reaction carried out in water. Besides the application as an efficient support, the water-dispersible Fe_3O_4 nanowire is also promising for other applications, such as biological sensing, labeling, and imaging.

Acknowledgements

This work was supported by the research fund of the National Natural Science Foundation of China (No. 21306132) and Doctoral Program of Higher Education (No. 20120032120008).

Notes and references

[a] Key Laboratory of Green Chemical Technology of Ministry of Education, Collaborative Innovation Center of Chemical Science and Engineering (Tianjin), School of Chemical Engineering and Technology, Tianjin University, Tianjin 300072, China

[b] College of Material Science & Chemical Engineering, Tianjin University of Science & Technology, Tianjin 300457, PR China

Electronic Supplementary Information (ESI) available: Scheme of the catalytic reduction reaction by $NaBH_4$ for the conversion of 4-NP to 4-AP; scheme of catalytic hydrogenation of 4-NP to 4-AP; photograph of as-synthesized Fe_3O_4 dispersed in H_2O; TEM image of Fe_3O_4 samples prepared by coprecipitation; EDS spectrum of Pd/Fe_3O_4 nanowire; EDS spectrum of Pt/Fe_3O_4 nanowire; typical TEM images of the as-synthesized Pd nanoparticles and Pt nanoparticles; catalytic activity for the reduction of 4-NP by H_2 in water at room temperature. See DOI: 10.1039/b000000x/

References

1. Y. Wang, Z. Xiao and L. Wu, *Curr. Org. Chem.*, 2013, **17**, 1325-1333.
2. N. T. Phan, C. S. Gill, J. V. Nguyen, Z. J. Zhang and C. W. Jones, *Angew. Chem. Int. Edit.*, 2006, **45**, 2209-2212.
3. M. Boudart, in *Advances in catalysis and related subjects*, ed. D. D. Eley, Academic Press, 1969, pp. 153-163.
4. B. C. Gates, *Chem. Rev.*, 1995, **95**, 511-522.
5. X. Y. Liu, A. Wang, T. Zhang and C.-Y. Mou, *Nano Today*, 2013, **8**, 403-416.
6. J. Nakamura and T. Kondo, *Top. Catal.*, 2013, **56**, 1560-1568.
7. K. Jia, H. Zhang and W. Li, *Chinese J. Catal.*, 2008, **29**, 1089-1092.
8. Z. Qiu, H. Huang, J. Du, T. Feng, W. Zhang, Y. Gan and X. Tao, *J. Phys. Chem. C*, 2013, **117**, 13770-13775.
9. M. Zhao and R. M. Crooks, *Angew. Chem. Int. Ed.*, 1999, **38**, 364-366.
10. J. Liu, *ChemCatChem*, 2011, **3**, 934-948.
11. P. X. Huang, F. Wu, B. L. Zhu, X. P. Gao, H. Y. Zhu, T. Y. Yan, W. P. Huang, S. H. Wu and D. Y. Song, *J. Phys. Chem. B*, 2005, **109**, 19169-19174.
12. J.-Y. Luo, M. Meng, H. Xian, Y.-B. Tu, X.-G. Li and T. Ding, *Catal. Lett.*, 2009, **133**, 328-333.
13. Y. Shen, G. Lu, Y. Guo, Y. Wang, Y. Guo, L. Wang and X. Zhen, *Catal. Commun.*, 2012, **18**, 26-31.
14. I. I. Soykal, B. Bayram, H. Sohn, P. Gawade, J. T. Miller and U. S. Ozkan, *Appl. Catal. A*, 2012, **449**, 47-58.
15. R. Gao, D. Zhang, P. Maitarad, L. Shi, T. Rungrotmongkol, H. Li, J. Zhang and W. Cao, *J. Phys. Chem. C*, 2013, **117**, 10502-10511.
16. X. Mou, B. Zhang, Y. Li, L. Yao, X. Wei, D. S. Su and W. Shen, *Angew. Chem. Int. Ed.*, 2012, **51**, 2989-2993.
17. Z. Zhong, J. Ho, J. Teo, S. Shen and A. Gedanken, *Chem. Mater.*, 2007, **19**, 4776-4782.
18. F. Wang, R. Shi, Z.-Q. Liu, P.-J. Shang, X. Pang, S. Shen, Z. Feng, C. Li and W. Shen, *ACS Catal.*, 2013, **3**, 890-894.
19. K.-W. Park, Y.-W. Lee, J.-K. Oh, D.-Y. Kim, S.-B. Han, A. R. Ko, S.-J. Kim and H.-S. Kim, *J. Ind. Eng. Chem.*, 2011, **17**, 696-699.
20. J. Rajeswari, B. Viswanathan and T. K. Varadarajan, *Mater. Chem. Phys.*, 2007, **106**, 168-174.
21. M. Zhu and G. Diao, *Phys. Chem. Chem. Phys.*, 2011, **115**, 24743-24749.
22. Lorenza Suber, Patrizia Imperatori, Giovanni Ausanio, Fabio Fabbri and H. Hofmeister, *J. Phys. Chem. B*, 2005, **109**, 7103-7109.
23. M. B. Gawande, P. S. Branco and R. S. Varma, *Chem. Soc. Rev.*, 2013, **42**, 3371-3393.
24. A. Yan, Y. Liu, Y. Liu, X. Li, Z. Lei and P. Liu, *Mater. Lett.*, 2012, **68**, 402-405.
25. I. Milosevic, H. Jouni, C. David, F. Warmont, D. Bonnin and L. Motte, *J. Phys. Chem. C*, 2011, **115**, 18999-19004.
26. Y. Tang and Q. Chen, *Chem. Lett.*, 2007, **36**, 840-841.
27. J. Zhang, J. Chen and Z. Wang, *Mater. Lett.*, 2007, **61**, 1629-1632.
28. S. Lian, E. Wang, L. Gao, Z. Kang, D. Wu, Y. Lan and L. Xu, *Solid State Commun.*, 2004, **132**, 375-378.
29. J. Wang, Q. Chen, C. Zeng and B. Hou, *Adv. Mater.*, 2004, **16**, 137-140.
30. N. Du, Y. Xu, H. Zhang, C. Zhai and D. Yang, *Nanoscale Res. Lett.*, 2010, **5**, 1295-1300.
31. Y. S. Kang, S. Risbud, J. F. Rabolt and P. Stroeve, *Chem. Mater.*, 1996, **8**, 2209-2211.
32. M. J. Harrington, A. Masic, N. Holten-Andersen, J. H. Waite and P. Fratzl, *Science*, 2010, **328**, 216-220.
33. H. Lee, S. M. Dellatore, W. M. Miller and P. B. Messersmith, *Science*, 2007, **318**, 426-430.
34. H. Deng, X. Li, Q. Peng, X. Wang, J. Chen and Y. Li, *Angew. Chem. Int. Ed.*, 2005, **117**, 2842-2845.
35. K. He, C.-Y. Xu, L. Zhen and W.-Z. Shao, *Mater. Lett.*, 2007, **61**, 3159-3162.
36. Z. Huang, Y. Zhang and F. Tang, *Chem. Comm.*, 2005, 342-344.
37. L. Guo, Q. Liu, G. Li, J. Shi, J. Liu, T. Wanga and G. Jiang, *Nanoscale*, 2012, **4**, 5864-5867.
38. B. Fei, B. Qian, Z. Yang, R. Wang, W. C. Liu, C. L. Mak and J. H. Xin, *Carbon*, 2008, **46**, 1795-1797.
39. K. R. Priolkar, P. Bera, P. R. Sarode, M. S. Hegde, S. Emura, R. Kumashiro and N. P. Lalla, *Chem. Mater.*, 2002, **14**, 2120-2128.
40. M. Brun, A. Berthet and J. C. Bertolini, *J. Electron. Spectrosc. Relat. Phenom.*, 1999, **104**, 55-60.
41. T. Pillo, R. Zimmermann, P. Steiner and S. Hüfner, *J. Phys.: Condens. Matter*, 1997, **9**, 3987.
42. P. Bera, K. R. Priolkar, A. Gayen, P. R. Sarode, M. S. Hegde, S. Emura, R. Kumashiro, V. Jayaram and G. N. Subbanna, *Chem. Mater.*, 2003, **15**, 2049-2060.

43. P. Hervés, M. Perez-Lorenzo, L. M. Liz-Marzan, J. Dzubiella, Y. Lu and M. Ballauff, *Chem. Soc. Rev.*, 2012, **41**, 5577-5587.
44. R. lmbihl and G. Ertl, *Chem. Rev.*, 1995, **95**, 697-733.
45. A. Corma and P. Serna, *Science*, 2006, **313**, 332-334.
46. F. Zhang, J. Jin, X. Zhong, S. Li, J. Niu, R. Li and J. Ma, *Green Chem.*, 2011, **13**, 1238-1243.
47. S. J. Hoseini, M. Rashidi and M. Bahrami, *J. Mater. Chem.*, 2011, **21**, 16170-16176.
48. S. Wunder, Y. Lu, M. Albrecht and M. Ballauff, *ACS Catalysis*, 2011, **1**, 908-916.
49. Y. Mei, Y. Lu, F. Polzer, M. Ballauff and M. Drechsler, *Chem. Mater.*, 2007, **19**, 1062-1069.
50. K. Esumi, R. Isono and T. Yoshimura, *Langmuir*, 2004, **20**, 237-243.
51. S. Harish, J. Mathiyarasu, K. L. N. Phani and V. Yegnaraman, *Catal. Lett.*, 2009, **128**, 197-202.
52. S. Behrens, A. Heyman, R. Maul, S. Essig, S. Steigerwald, A. Quintilla, W. Wenzel, J. Bürck, O. Dgany and O. Shoseyov, *Adv. Mater.*, 2009, **21**, 3515-3519.
53. A. Halder, S. Patra, B. Viswanath, N. Munichandraiah and N. Ravishankar, *Nanoscale*, 2011, **3**, 725-730.
54. R. Bhandari and M. R. Knecht, *ACS Catalysis*, 2011, **1**, 89-98.
55. S. Arora, P. Kapoor and M. Singla, *Reac Kinet Mech Cat*, 2010, **99**, 157-165.
56. J. Yuan, S. Wunder, F. Warmuth and Y. Lu, *Polymer*, 2012, **53**, 43-49.
57. J. A. Johnson, J. J. Makis, K. A. Marvin, S. E. Rodenbusch and K. J. Stevenson, *J. Phys. Chem. C*, 2013, **117**, 22644-22651.
58. T. Yao, T. Cui, X. Fang, F. Cui and J. Wu, *Nanoscale*, 2013, **5**, 5896-5904.
59. X. Lu, X. Bian, G. Nie, C. Zhang, C. Wang and Y. Wei, *J. Mater. Chem.*, 2012, **22**, 12723-12730.
60. B. Liu, S. Yu, Q. Wang, W. Hu, P. Jing, Y. Liu, W. Jia, Y. Liu, L. Liu and J. Zhang, *Chem. Commun.*, 2013, **49**, 3757-3759.
61. Y. Mei, G. Sharma, Y. Lu, M. Ballauff, M. Drechsler, T. Irrgang and R. Kempe, *Langmuir*, 2005, **21**, 12229-12234.
62. J. Yuan, F. Schacher, M. Drechsler, A. Hanisch, Y. Lu, M. Ballauff and A. H. E. Müller, *Chem. Mater.*, 2010, **22**, 2626-2634.
63. P. Das, T. Heuser, A. Wolf, B. Zhu, D. E. Demco, S. Ifuku and A. Walther, *Biomacromolecules*, 2012, **13**, 4205-4212.
64. H. Li, J. Lü, Z. Zheng and R. Cao, *J. Colloid Interface Sci.*, 2011, **353**, 149-155.
65. A. M. Kalekar, K. K. K. Sharma, A. Lehoux, F. Audonnet, H. Remita, A. Saha and G. K. Sharma, *Langmuir*, 2013, **29**, 11431-11439.

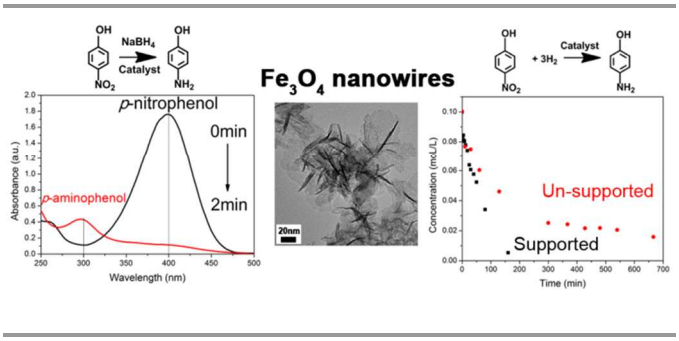

Table of contents